2019

PROPERTIES AND APPLICATIONS OF TETRAALKYLPHOSPHONIUM ALKYLSULFATE IONIC LIQUIDS AND 3D PRINTED POLYMERIZED IONIC LIQUIDS

Mustafa Mohammed Alhussain
Murray State University

Recommended Citation

Alhussain, Mustafa Mohammed, "PROPERTIES AND APPLICATIONS OF TETRAALKYLPHOSPHONIUM ALKYLSULFATE IONIC LIQUIDS AND 3D PRINTED POLYMERIZED IONIC LIQUIDS" (2019). *Murray State Theses and Dissertations*. 158.
https://digitalcommons.murraystate.edu/etd/158

PROPERTIES AND APPLICATIONS OF TETRAALKYLPHOSPHONIUM ALKYLSULFATE IONIC LIQUIDS AND 3D PRINTED POLYMERIZED IONIC LIQUIDS

A Thesis
Presented to the
Faculty of the Department of Chemistry
Murray State University
Murray, Kentucky

In Partial Fulfillment of the
Requirements for the Degree of
Master of Science

By
Mustafa Mohammed Alhussain
December 2019

PROPERTIES AND APPLICATIONS OF UNIQUE IONIC LIQUIDS AND POLYMERIZED IONIC LIQUIDS

DATE APPROVED: ________________

Thesis Advisor

Member, Thesis Committee

Member, Thesis Committee

Member, Thesis Committee

Collegiate Graduate Coordinator

Dean of College

Graduate Studies Coordinator

Provost

ACKNOWLEDGEMENTS

I sincerely offer a deep sense of gratitude to Dr. Daniel Johnson of the Murray State Chemistry Department for his exceptional assistance, invaluable supervision, and guidance. This work is the result of his extraordinary and generous attitude. I am especially grateful to Dr. Kevin Revell and Dr. Kevin Miller for their continuous support, advice, and patience during the process of this work. I would like to thank the faculty of the Chemistry Department for their valuable comments and suggestions throughout my journey at Murray State University. To my kids Joory and Qassim, all family members, relatives, and friends who in one way or another shared their support, constructive discussion, valuable perspective, and encouragement during this work, thank you.

ABSTRACT

Ionic liquids (ILs) are defined as pure salts with a melting temperature below 100 °C with a subset called room-temperature ILs (RTILs) with melting temperatures at or below room temperature. The sizes of the cation and anion play a critical role in determining the properties, with smaller ions forming stronger ionic forces and packing better, raising viscosity and lowering conductivity of the IL. At the same time, intermolecular forces such as van der Waals and hydrogen bonding can play a role in IL properties as well. Our research described herein is focused on three tetraalkylphosphonium-based cations coupled with three alkylsulfate anions, all containing different alkyl chain lengths. Changes in physicochemical properties as a function of changing alkyl chain length were investigated (i.e. van der Waals forces) across all nine possible IL combinations.

Specifically, studies were focused on conductivities, viscosities, and densities. In general, the purity of the synthesized ILs was estimated to be above 98%. In the case of density, ILs with the smallest cation (tbP^+) family had the highest density, while the largest cation family demonstrated the lowest density, with the trend as follows: $tbP^+ > tbtdP^+ > thtdP^+$. With viscosity, a slightly different trend was observed; the $tbtdP^+$ cation family had the highest viscosity among the three, followed by TdP^+ then $thtdP^+$. The change in pattern could be due to the impact of not just size/packing and ionic forces but also van der Waals forces. Conductivity was highest for the smallest ILs (tbP^+) while the lowest conductivity was reported for the largest IL ($thtdP^+$). Within the same cation group higher conductivity was measured for the smallest anion size in the order of $ds^- > dds^- > tds^-$.

Polymerized ionic liquids, or poly ILs, are a special type of polyelectrolyte that contains a monomeric IL species in the repeating unit. Different polymer synthetic methods have been applied to create PILs; however, thiol-ene ‘click’ photopolymerization offers a solventless, rapidly-curing platform for the preparation of homogenous polymer networks. In the second study, a tetrafunctional thiol, pentaerythritol tetrakis (3-mercapto-propionate) (PTMP), was reacted with a bifunctional ionic liquid ene, 1,3-bisallylimidazolium (NTf_2) to form polyIL networks. In the particular project described herein, the aforementioned advantages of thiol-ene photopolymerization was utilized in stereolithographic (SLA) 3D printing. However, the initial resolution of the printed pieces was not satisfactory due to light scattering within the neat thiol-ene resin. For this reason, further steps to improve the resolution were taken by adding an absorptive, anti-scattering material (Sudan I) to the thiol-ene resins.

The impact of Sudan I addition at various weight percents on thermal, mechanical, and conductive properties, as well as thiol-ene curing rate, were examined. Thiol-ene photopolymers were prepared in two ratios: 1.0:1.0, and 1.0:2.0 (corresponding to the thiol:ene mol ratio) with different weight percents (0.02%, 0.05%, 0.10%) of Sudan I dye for each ratio. Thermal, mechanical, and conductive properties for both 3D printed, and UV lamp cured parts were tested to measure any differences in properties. In general, the type of curing and addition of Sudan I to the resin did not significantly change the thermal stability of the polymer. The conductivity of the different polymer compositions including UV cured, 3D printed, and the additions of both 0.02% and 0.05% Sudan I were measured, and the results were nearly identical. For evaluating resolution, squares of know dimensions were printed and actual and specified dimensions were computed. A 1:2 thiol-ene containing no Sudan were between 20 - 28% bigger than specified (“overgrowth”), while the same 1:2 polymer containing 0.02% Sudan showed improved resolution with between 12 and 17% overgrowth.

TABLE OF CONTENTS

LIST OF FIGURES

LIST OF TABLES

CHAPTER ONE

INTRODUCTION

1. Ionic Liquids

Ionic liquid (ILs) are defined as salts with a melting temperature below 100 °C with a subset called room-temperature ILs (RTILs) with melting temperatures at or below room temperature.[1] In the past couple of decades, ILs have experienced exponential growth in different areas due to their properties and variety of applications. ILs have unique physicochemical properties, including nonflammability, high ionic conductivity, wide liquid temperature ranges in conjunction with thermal stability, highly concentrated ionic atmosphere, and negligible vapor pressure.[2] Therefore, they have been considered a replacement for organic solvents used in chemical catalytic reactions, purification, and separation.[3] In addition, they are considered novel organic and inorganic reaction media and separation solvents.[1] Furthermore, RTILs are very common in electrochemistry applications, such as lithium ion batteries, dye-sensitized solar cells, capacitors, and exchange membrane.[4]

The wide variety of cation and anion combinations allows significant flexibility in material design and in the optimization of properties for specific applications.[5] Examples of common cations used include imidazolium, pyridinium, pyrrolidinium, ammonium, sulfonium and phosphonium derivatives (Figure 1-1).[1] Common anions that have been used are halides (Cl, Br, and I), alkyl sulfonates, carboxylates, fluorinated organics, dicyanamide, and nitrate. The combination of cation and anion can have a substantial impact on the properties of the resulting ILs. For example, chloride is significantly smaller than an alkyl sulfonate, which reduces space between cation and anion, yielding stronger ionic interactions and better ion packing. Stronger ionic forces and improved packing then lead to raised phase transition temperatures, increased viscosities, reduced conductivity, etc. Of course, other intermolecular forces such as van der Waals and hydrogen bonding can play a role in IL properties as well. Furthermore, Lewis acidity/basicity of the ions also impact ionic interactions.[1] Most of the cations used in ILs, then, are relatively bulky, often asymmetric, organic compounds that will inhibit the ability to form strong ionic interactions with anions and reduce packing ability. In addition, many ILs contains both bulky cations and anions that result in further reduction in ionic interactions and packing.

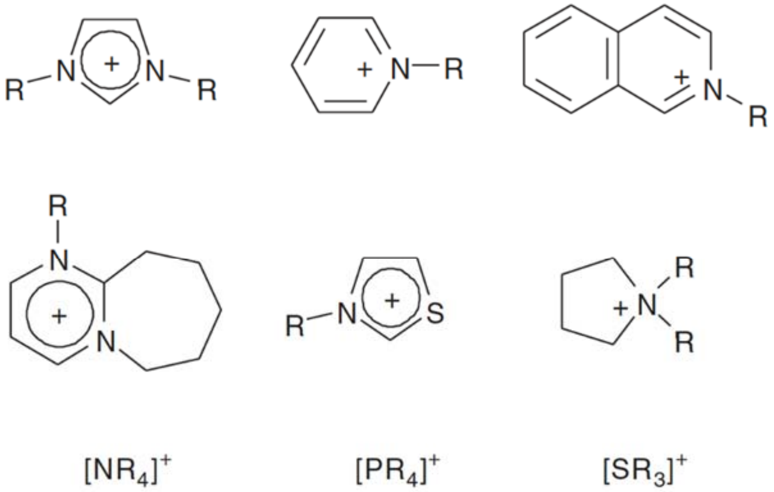

Figure 1-1: Examples of cations commonly used for the formation of ionic liquids.[1]

The research described herein is focused on tetraalkylphosphonium-based cations coupled with alkylsulfate anions, specifically those prepared from:

trihexyltetradecylphosphonium chloride ([thtdP^{+}][Cl^{-}]), tributyltetradecylphosphonium chloride ([tbtdP^{+}][Cl^{-}]), tetrabutylphosphonium chloride ([tbP^{+}][Cl^{-}]), sodium decylsulfate ([Na^{+}][ds^{-}]), sodium dodecylsulfate ([Na^{+}][dds^{-}]), and sodium tetradecylsulfate ([Na^{+}][tds^{-}]) (Figure 1-2). The relative impact of ionic and van der Waals forces on the ionic liquid properties are of primary interest. We investigated changes in physicochemical properties as a function of changing alkyl chain length across all nine possible IL combinations. Specifically, studies were focused on conductivity, viscosity, and density, as well as a cumulative determination of "ionicity". Previous work had already been performed in our lab to evaluate the thermal properties of these ILs (phase transitions and stability).

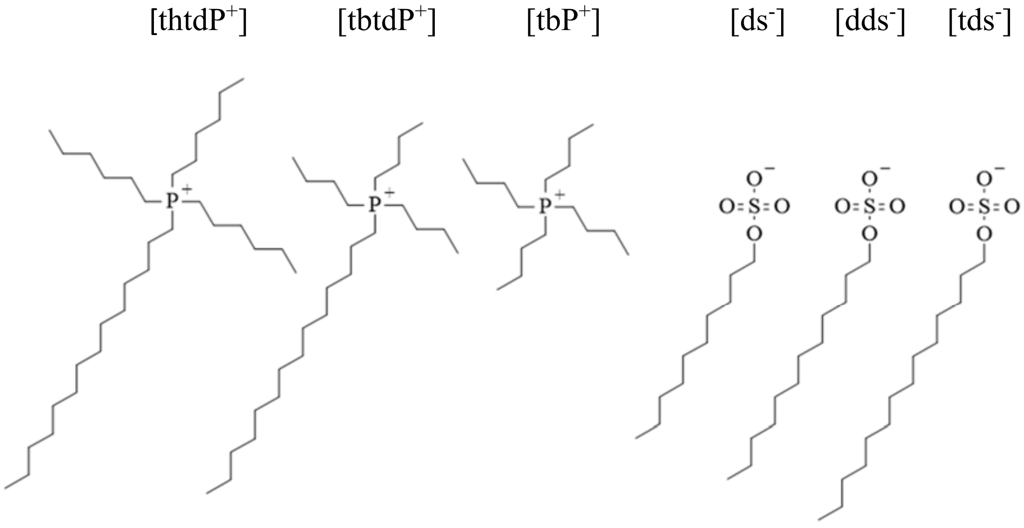

Figure 1-2: Structures of cations and anions used in the preparation of ILs.

2. Polymerized Ionic Liquids

Polymerized ionic liquids, or poly ILs, are a special type of polyelectrolyte that contain a monomeric IL species in the repeating unit.[6] Like ILs, a variety of cation and anion combinations are possible in PILs, giving them the unique properties of ILs, but with enhanced mechanical stability. Therefore, PILs have been proposed for a wide range of applications, as well, especially where conductive behavior and mechanical stability are needed simultaneously, such as: fuel cells, batteries, and electrolyets.[7] There is generally a reduction of conductivity in PILs compared to analogous ILs, due to one ion being immobilized in the polymer backbone,[8] with only the counterion mobile, i.e., PILs are single-ion conductors.

Different polymer synthesis methods have been applied to create PILs,[9] but the thiol-ene 'click' photopolymerization synthetic method offers a solventless, rapidly-curing platform for the preparation of homogenous polymer networks.[6] Ionic liquids can undergo thiol-ene radical polymerization, when the ionic liquid contains either a thiol or ene group. Such thiol-ene reactions could be initiated by either photochemistry or thermal conditions. The Hawker group has studied both conditions and concluded that the photochemical approach leads to faster, and more quantitative reactions in most cases.[12,13]

The general mechanism of photopolymerization, then, involves adding a photoinitiator to a mixture of thiol and ene monomers.[14] By applying a proper wavelength, the photoinitiator decomposes into a radical species that reacts with the thiol group to form a thiyl radical. In the presence of an ene-containing molecule, the thiyl radical reacts with the ene to obtain a carbon radical. The carbon radical abstracts a hydrogen from another thiol-containing molecule resulting in formation of second, new, thiyl radical (Figure 1-3). From there, the process repeats until the limiting reagent (which can be either thiol or ene) is consumed. Furthermore, the molar ratios of thiol and ene influences the extent of crosslinking in the resulting polymer.

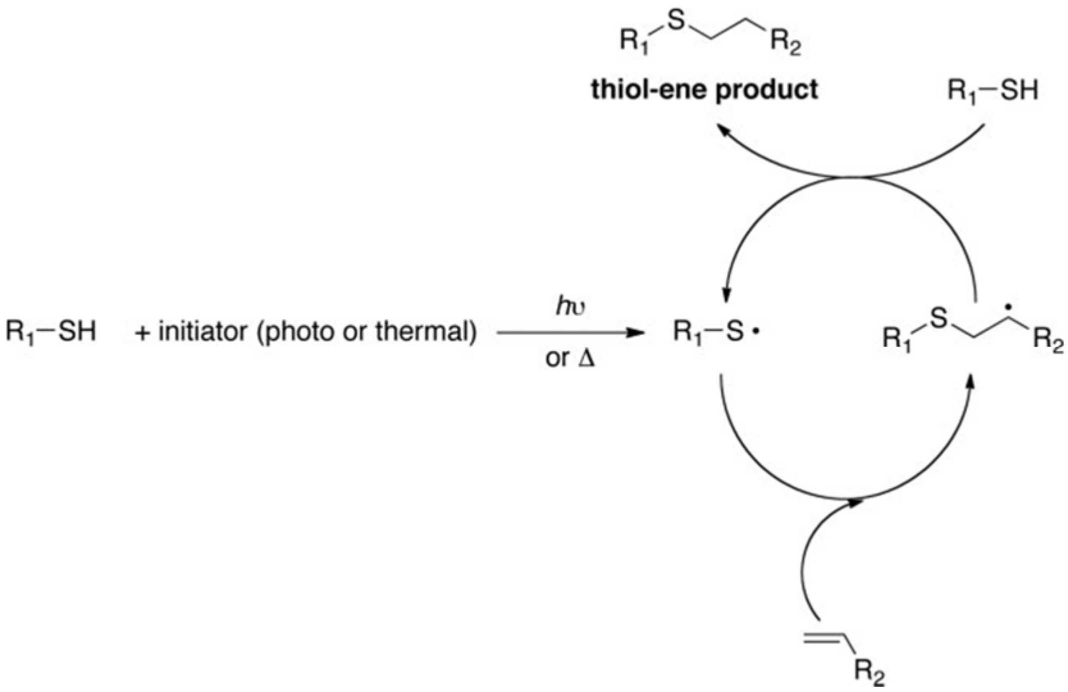

Figure 1-3: A general mechanism for the thiol-ene photopolymerization.[12]

In our study, a tetrafunctional thiol, pentaerythritol tetrakis(3-mercapto-propionate) (PTMP) was reacted with a bifunctional ionic liquid ene, 1,3-bisallylimidazolium [NTf_2] (Figure 1-4). Therefore, the stoichiometric equivalence for PTMP and 1,3-bisallylimidazolium [NTf_2] would be 1:2. However, other molar ratios are possible; Miller, et al. at Murray State have reported in a recent work crosslinked networks with different thiol:ene molar ratios (1.0:1.0, 1.0:1.5, 1.0:2.0, 1.0:2.5, and 1.0:3.0).[6] They showed that varying the molar ratio can change the thermal, mechanical and conductive properties. Due to its uniqueness of and control over properties, this family of photopolymerized networks can be utilized in a variety of applications, and is being studied in lithium ion batteries, ion sensors, gas separations, and for microfabrication in our lab. In particular, the rapid photocuring of the thiol-enes networks makes them potentially attractive in stereolithographic 3D printing.

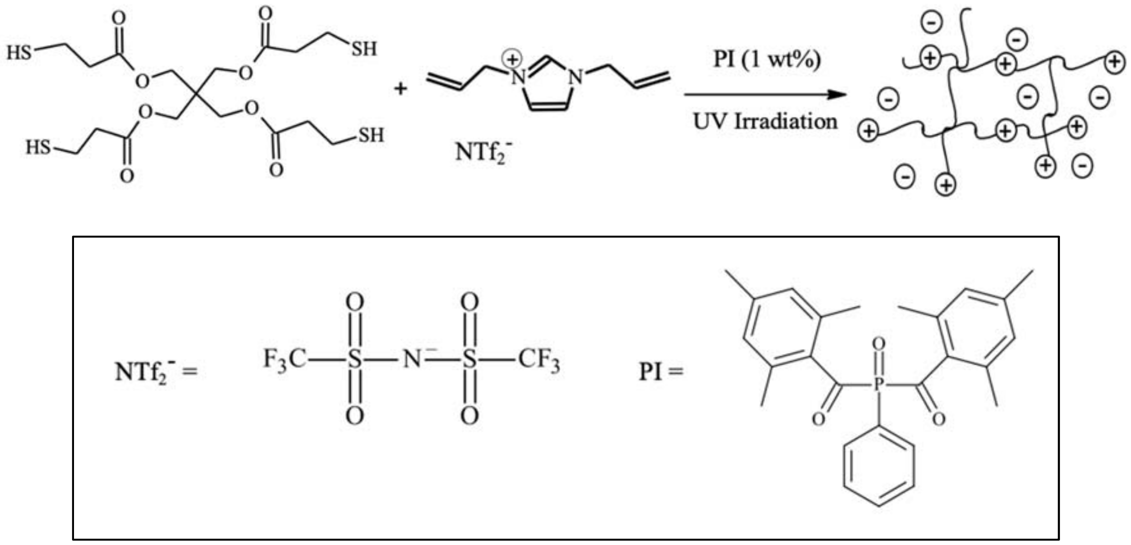

Figure 1-4: Network structure formed from photopolymerization between PTMP and bisallylimidazolium [NTf_2].

3. Three-Dimensional Printing

Additive manufacturing or three-dimensional printing (3D printing) has been growing exponentially in the past years because it allows the production of customized parts from metals, ceramics, and polymers without the need for molds or machining typical of formative and subtractive fabrication.[15] Some reasons for the fast growth in 3D printing technology include reduced production times, material efficiency, and low cost. Furthermore, 3D printing technology can allow the manufacture of more complex objects than these other technologies in a wide array of applications. For instance, many articles have been published recently where 3D printing was used for microfluidics and labs-on-a-chip,[15] electrochemical devices,[16] tissue engineering,[17] biology,[18], medicine,[19] and custom chemical labware.[20] 3D printing is a generic term for a variety of techniques and methods including stereolithography (SLA), selective laser sintering (SLS), inkjet and polyjet printing, fused deposition modeling (FDM), and laminated object manufacturing (LOM).[15]

In the particular project described herein, we utilized the aforementioned thiol-ene photopolymerization in stereolithographic (SLA) 3D printing. The SLA 3D printer includes a tank to contain a photocurable resin, movable build platform, and a light source (usually a 405 nm laser).[21] SLA 3D printing exists in two forms: free surface and constrained surface configurations, both consisting of the same basic elements. In the free surface configuration, the light source is mounted above the resin tank and polymerization occurs in layers that stack on top of each other, and the height of the resin reservoir determines the height of the printed product. On the other hand, in the constrained surface configuration, polymerization occurs at the bottom of the resin reservoir through a transparent window. This configuration has a movable platform that moves up in small increments as each layer is fully cured, and the process is repeated. One major advantage of this configuration is that this method does not depend on the height of the resin, which is important if an expensive or small quantity of resin must be used. In our study, we used a FormLabs Form 1+ 3D Printer that employed the constrained surface configuration (details about the operation of this, and other SLA printers, can be found at the FormLabs website, www.formlabs.com).

There are four requirements that the thiol-ene resin must have to qualify as a SLA 3D printing material. The resin must undergo photopolymerization at the wavelength of the laser in the printer, in our case 405 nm. Also, the curing rate of the resin must be relatively fast due to short exposure times in the printer. In addition, the cured layers must adhere to one another. Lastly, the resin must adhere more greatly to the aluminum build platform than the PDMS bottom of the resin tank. Previous preliminary work performed by our group showed that thiol-ene poly(ILs) containing PTMP, bisallylimidazolium NTf_2, and a phosphine oxide-based photoinitiator could be successfully employed as a 3D printing resin.[22] However, the resolution of the printed pieces was not satisfactory due to the light scattering within the thiol-ene resin. For this reason, we were motivated to take further steps to improve the resolution by adding an absorptive, anti-scattering material (Sudan I, Figure 1-5) to the thiol-ene resins. Sudan I was chosen as an additive to absorb scattered laser light and improve resolutions. Sudan I absorbs strongly at 405 nm, which make it suitable anti-scattering agent.[23] The impact of Sudan I addition at various weight percent on thermal, mechanical, and conductive properties, as well as the thiol-ene curing rate, were examined and are detailed in this thesis.

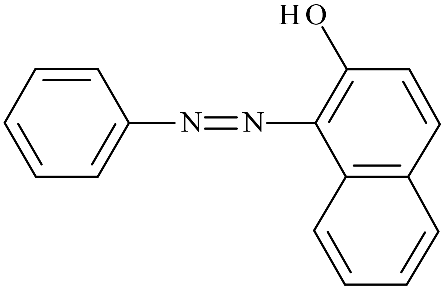

Figure 1-5: Sudan I chemical structure.

CHAPTER TWO

EXPERIMENTAL

1. Preparation and Characterization of Tetraalkylphosphonium Alkylsulfate Ionic Liquids

1.1 Materials

All of the following chemicals were purchased from Sigma-Aldrich and were used without further purification: trihexyltetradecylphosphonium chloride ([thtdP$^+$][Cl$^-$]), tributyltetradecylphosphonium chloride ([tbtdP$^+$][Cl$^-$]), tetrabutylphosphonium ([tbP$^+$][Cl$^-$]), sodium decylsulfate ([Na$^+$][ds$^-$]), sodium dodecylsulfate ([Na$^+$][dds$^-$]), sodium tetradecylsulfate ([Na$^+$][tds$^-$]). Dichloromethane (HPLC/UV grade) was obtained from Pharmco-Aaper, and deionized water (18 MΩ) was obtained from a Thermo Scientific™ Barnstead™ E-Pure™ Ultrapure Water Purification System.

1.2 Preparation and Purification of ILs

Each phosphonium cation was coupled with each alkylsulfate anion, resulting in a total of nine different ionic liquids. A previously published procedure was followed.[1] As an example, a molar excess of sodium decylsulfate (2.00 g, 1.2 molar equivalents) was combined with trihexyltetradecylphosphonium chloride (3.00 g, 1.0 molar equivalents) in a 100 mL round-bottomed flask. Into the round-bottomed flask, 30 mL of dichloromethane was added, and the solution was stirred for 48 hours while covered with aluminum foil to prevent any light exposure. After the reaction was completed, the mixture was filtered using 0.22 µm Durapore® membrane filters under vacuum to remove the sodium chloride and residual solid reactants. The resulting solution was washed three times with 50 mL aliquots of deionized water in a 250 mL glass separatory funnel; the organic layer containing the ionic liquid was collected while the aqueous layers were discarded. A rotary evaporator was then used to remove the dichloromethane solvent at 60 ºC under vacuum. Then, the ionic liquid was transferred to a small vial for further purification. The vial was held under high vacuum while submerged in an oil bath at 70 ºC for 72 hours to remove trace water and dichloromethane. All glassware used in this procedure was washed with water, acetone, ethanol, and dried with nitrogen gas. Finally, the purified ionic liquid product was stored in a vacuum desiccator when not in use.

1.3 Evaluation of Purity by Ion Chromatography and Nuclear Magnetic Resonance Spectroscopy

^{1}H NMR spectra were measured on a JEOL-ECS 400 MHz NMR. For each measurement, 10 – 30 mg of the purified ionic liquid was placed into an NMR tube and dissolved in chloroform-*d*. In a perfectly pure IL sample, an alpha proton ratio of 8:2 between the cation and anion, respectively, should be obtained (phosphonium alpha protons appear at 2.26 ppm, while alkylsulfate alpha protons appear at 3.98 ppm). The quantity of chloride ion impurity in the synthesized ILs was measured by a Dionex ICS-1100 ion chromatograph. A series of standards was prepared using a 100 ppm multielement anion stock solution obtained from High-Purity Standards. In general, the chromatography showed that all ILs contained <100 ppm of residual chloride.

1.4 Measurement of Physicochemical Properties of the ILs

A custom-built (in-house) electrode cell was designed as shown in Figure 2-1 to test the conductivity of the synthesized ionic liquids. A Swagelok ¼” stainless steel Ultra-Torr tee was used as the base of the cell. A platinized Pt 2-electrode cell was attached to one side of the tee with both a Viton® O-ring and threaded PTFE O-ring. On a second arm of the tee was attached a drying tube that contained anhydrous calcium chloride. The third opening of the union tee was blocked with ¼” diameter PTFE piece. Approximately 0.5 mL of the IL was added prior to attaching the drying tube to the union tee. The cell was positioned in an aluminum block that was taped with aluminum tape to a digital hot plate. The conductivity of ILs was measured over a range of temperatures from 25 to 80 ºC in 5 ºC increments, with a thermocouple contacting the sample to ensure temperature accuracy. In addition, the conductivity cell was calibrated with 20 mM and 200 mM KCl standards, and the cell constant was obtained before any IL measurement. The cell constant was used to convert measured conductance (S) to conductivity (S/cm). Conductance was monitored by computer through an eDAQ Conductivity isoPod EPU357.

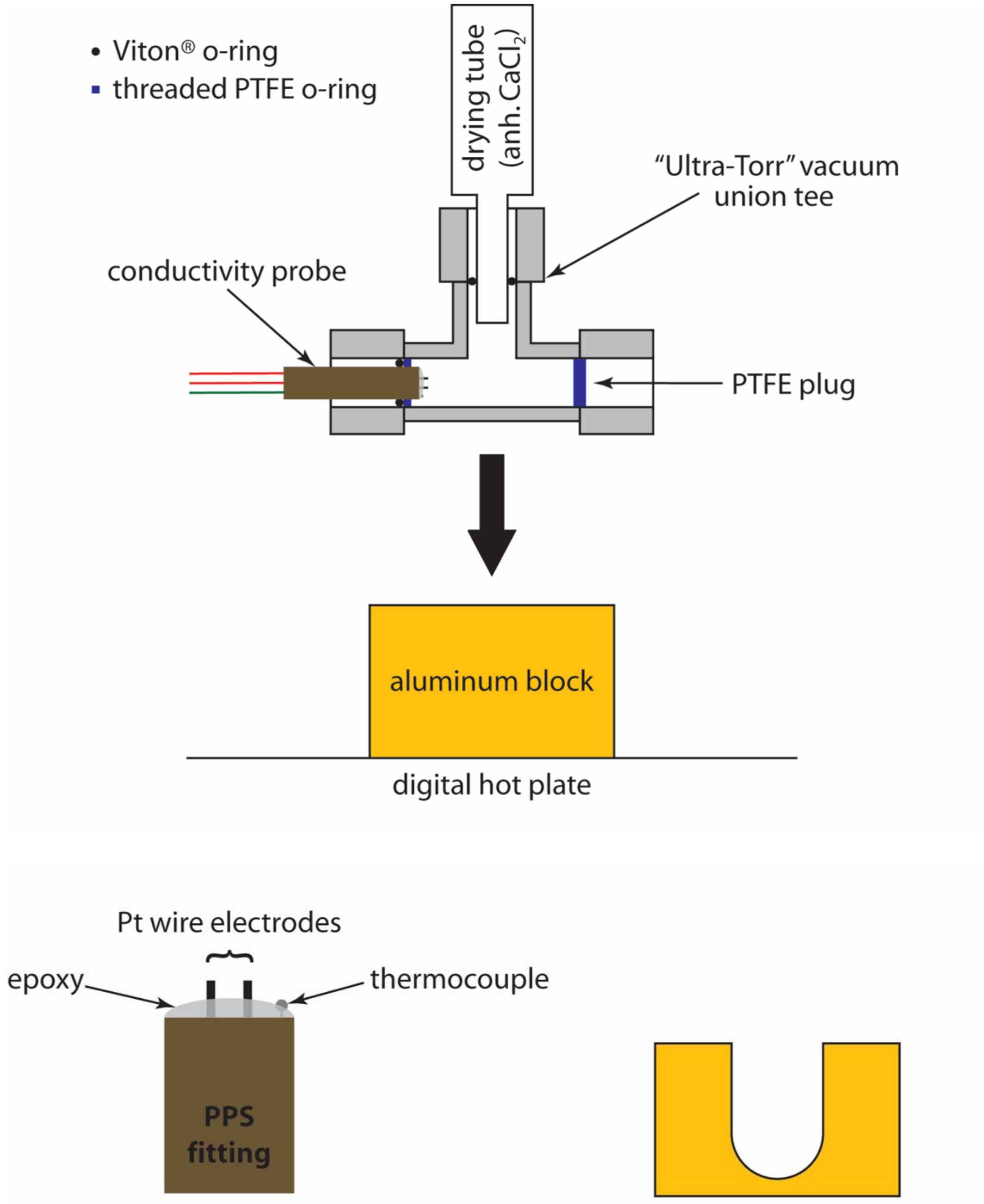

a. enhanced view of probe tip

b. side view of aluminum block

Figure 2-1: The top diagram shows the assembly of the custom-built electrode cell: a) enhanced view of probe tip that shows the platinized Pt electrodes and thermocouple held together by epoxy in a poly (phenylene sulfide) (PPS) fitting. b) a side view of the aluminum block where the electrode cell was placed during measurement.

To determine viscosity of the ILs approximately 0.5 mL of ionic liquid was placed in parallel-plate Brookfield Viscometer model DV2T. Viscosity was measured over a temperature range from 25 to 80 ºC in 5 ºC increments. There was a 45 minute delay between each measurement to ensure the sample had equilibrated at the desired temperature. Density was measured using an Anton Paar DMA 4100 M density meter in the 25 - 80 ºC temperature range in 5 ºC increments. The density meter was calibrated by measuring densities of air and deionized water at 25 ºC before use.

2. Evaluation of Thiol-ene Poly(ILs) as 3D Printing Materials

2.1 Materials

The following chemicals were purchased from Sigma-Aldrich: phenylbis(2,4,6-trimethylbenzoyl)phosphine oxide (PI), pentaerythritol tetrakis(3-mercapto-propionate) (PTMP, > 95%), Sudan I dye (≥95.0%), and ethyl acetate. The 1,3-bisallylimidazolium [NTf_2] ionic liquid monomer was synthesized by and obtained from the lab of Dr. Kevin Miller of Murray State University; it was synthesized according to a previously published procedure.[4] Deionized water (18 MΩ) was obtained from a Thermo Scientific™ Barnstead™ E-Pure™ Ultrapure Water Purification System.

2.2 Preparation of Poly(ILs) Monomer Solutions

For the purposes of this research, thio-lene photopolymer networks were prepared using two ratios, 1.0:1.0 and 1.0:2.0 (corresponding to the thiol:ene mol ratio), with a different weight percent (0.02%, 0.05%, 0.10%, 0.20%) of Sudan I dye for each ratio. Sudan I was dissolved in ethyl acetate in a glass vial, covered with aluminum foil to minimize light exposure, to create a 10 mg/mL stock solution. Then, the Sudan I solution was mixed with a proper amount of 1,3-bisallylimidazolium [NTf_2] ionic liquid. This mixture was placed in a 60 ºC vacuum oven for 24 hours to remove ethyl acetate.

In another glass vial, the desired amount of pentaerythritol tetrakis(3-mercapto-propionate) (PTMP) was mixed with phenylbis(2,4,6-trimethylbenzoyl)phosphine oxide (PI) photoinitiator, and the mixture was gently heated by a heat gun and shaken by hand until PI had completely dissolved. The vial was wrapped with aluminum foil to minimize exposure to stray light and was kept in a dark place to cool to room temperature. (Note: the PI was added to obtain 1% wt relative to total the final monomer solution mass.) The proper amount of 1,3-bisallylimidazolium [NTf_2]/Sudan I was added to the PTMP/PI mixture, the mixture was vortexed until homogenous, and allowed to set for 5 - 10 minutes to remove bubbles.

2.3 Measurement of Polymer Curing Rate

At this point, the monomer mixture was used in a number of ways: laser curing tests, photorheology, 3D printing and standard UV lamp curing. The last two are discussed in later sections. All tests were performed in a darkened room. For laser-based analysis of cure rate and depth, a flat PTFE piece with six 4-mm holes was clamped with binder clips to a silanized glass slide. A Free Mascot 50 mW, 405-nm laser pointer was clamped pointing down toward the holes. A manual shutter was positioned between the laser and the holes. PIL was added to fill each hole, and the holes were exposed to the laser for approximately 0.5, 1.0, 1.5, 2.0, 3.0, and 4.0 seconds. This exposure test was recorded by high frame rate (USB) video camera and the actual exposure times were determined to within ±0.025 seconds using video playback. Immediately after the experiment was completed, cured PIL pieces were washed with isopropyl alcohol and acetone to remove unreacted material. The dimensions corresponding to cure depth of the cured pieces were measured under microscope using an image analysis micrometer slide (Edmund Optics 53-713).

A TA Instruments Discovery Hybrid Rheometer HR-2 equipped with UV curing accessory was used to test the curing of Sudan I containing polymer at lamp intensities of 22.6 and 4.5 mW/cm^2. Lamp intensities were calibrated with a Silver Line UV Radiometer and, before adding the sample, the rheometer gap was zeroed. Then, a sample (~ 100 µL) was added to the 20-mm diameter quartz plate and the gap was set to 200 µm. Elastic and viscous moduli (storage and loss modulus) were obtained for 60 s before and for 300 s after light exposure.

2.4 Polymer Cured by UV Lamp

For standard lamp curing, approximately 1.0 gram of poly IL monomer mixture was prepared and placed into a 1” square mold based on a PTFE spacer with a thickness of approximately 0.5 mm sandwiched between two silanized glass slides. The mixture was cured by placing the filled mold under broadband ultraviolet radiation from a 100 W (8500 lumen) Longwave B-100 series UVP Mercury Spot Lamp (UVP, LLC; Upland, CA), for 10-20 minutes on each side (depending on the percentage of Sudan I in the sample). The cured square sample film was placed in a 60 ºC vacuum oven for 24 hours to remove trace amounts of water and volatiles. After complete drying of the square sample film, a clean razor blade and cork borer was used to cut pieces for testing by DSC, TGA, DMA, and DRS.

2.5 3D Printing

The preparation of the poly IL occurred as discussed earlier but on a larger scale. An approximately 100 g batch of thiol-ene resin was placed in a clean resin tank of the FormLabs Form 1+ 3D Printer. A series of shapes as shown in Figure 2-2 were designed in a computer-aided modeling program and converted to a .stl file. The file was sent to the printer and the desired layer thickness (0.05 mm) and scan rate (FormLabs setting for "Clear Resin Version 2") were selected. When printing was completed, the pieces were removed from the aluminum build platform and immediately washed thoroughly with isopropyl alcohol. For further washing the pieces were submerged in isopropyl alcohol and sonicated for 10 minutes to removed unreacted material. Then, the pieces were placed in a vacuum oven at 60 ºC for 24 hours to remove trace amounts of water and volatiles. The thermal, mechanical, and conductive properties were tested, as with lamp cured pieces, according to details discussed in the next section. 3D printed pieces were also subjected to size measurement to evaluate similarity between specified and actual printed size.

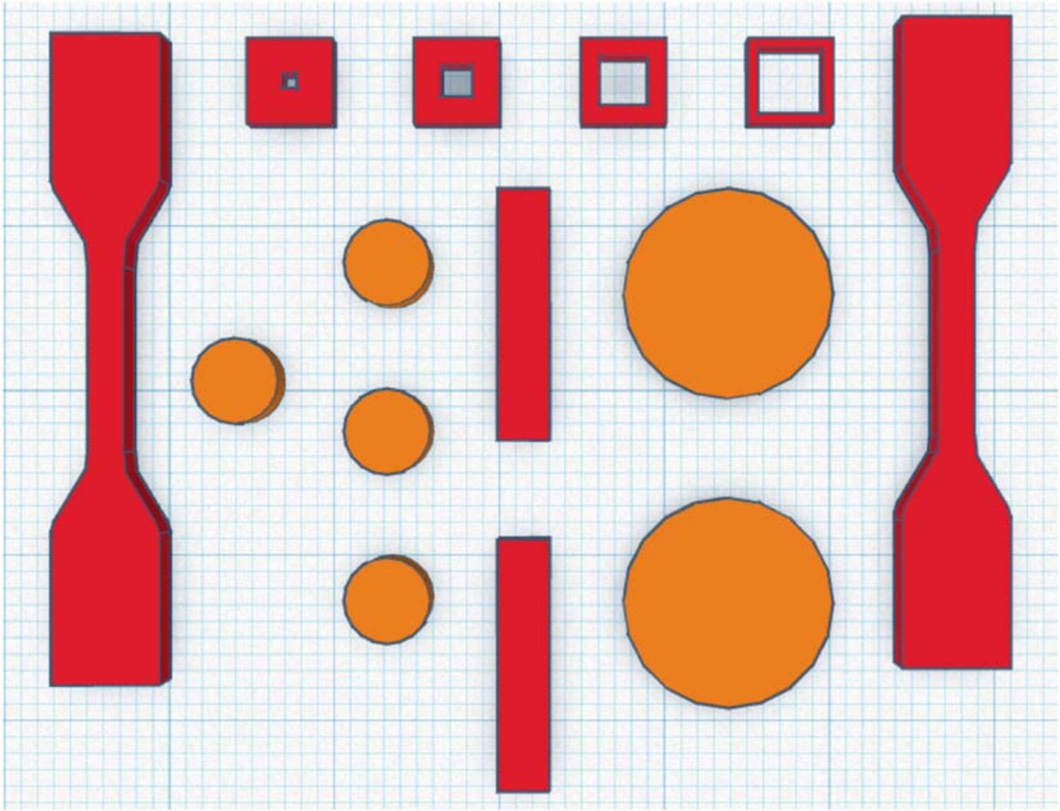

Figure 2-2: Design of different shapes printed in the FormLabs 3D printer. The 4 squares were used to evaluate resolution, 4 small discs were used in TGA/DSC measurements, 2 large cylinders were used in DRS, and the two rectangular strips employed for DMA.

2.6 Thermal, Mechanical and Conductivity Property Assessment

To determine the thermal stability of the thiol-ene polymers containing Sudan I, a TA Instruments Q500 thermogravimetric analyzer (TGA) was used. A sample (5-10 mg) was placed in a tared platinum pan and heated from 30 to 1000 °C at 10 °C/min under flow of dry nitrogen (35 mL/min). The onset of thermal decomposition (T_{onset}) was determined from the intersection of the tangents of the beginning and sloped portions of the TGA curve. In addition, $T_{d5\%}$ was determined as the temperature at which 5% weight loss was observed.

The glass transition temperature (T_g) for each thiol-ene polymer containing Sudan I was measured using a TA Instruments Q200 differential scanning calorimeter (DSC). Measurements were performed under a 50 mL/min flow of dry nitrogen. A sample (10-15 mg) was placed in a sealed aluminum pan, which initially was equilibrated at - 90 ºC, followed by heating to 150 ºC at a rate of 5 ºC/min. This heating cycle was repeated and the T_g measurement was obtained from the second heating event using half extrapolated tangents method.

A TA Instruments Q800 dynamic mechanical analyzer (DMA) was used to determine the mechanical properties of the thiol-ene polymer containing Sudan I. A rectangular piece with approximately 0.5 mm thickness was cut using a clean razor blade to dimensions of 10 mm x ~2 mm (the actual thickness and width were measured by a digital caliper for each sample). The sample strip was mounted in the tensile tension clamp of the DMA. Modulus measurements were performed over a temperature range of -90 to 150 ºC with a 5 ºC/min temperature ramp under a dry nitrogen environment. Oscillation of the tensile stress on the polymer occurred at a constant amplitude (1 μm) and frequency (1 Hz).

A custom built (in-house) two electrode cell (Figure 2-3) connected to a Metrohm FRA32M frequency response analyzer was used to measure conductivity by dielectric relaxation spectrometry (DRS). The two electrodes were polished with 0.50, 1.0, 2.0, and 4.0-micrometer diamond paste (Sandvik Hyperion; Worthington, Ohio) before they were used. A PIL sample with approximately 12.5 mm diameter and 0.5 mm thickness was placed in the middle of a PTFE 0.5 mm spacer that was sandwiched between the two electrodes. Electrodes and sample were further sandwiched between PTFE mounts and two stainless steel caps. Six 4-40 bolts and nuts were used to tighten the cell to 3 in-lb with a torque driver. Then the cell was placed into an ESPEC BTU-433 controlled temperature and humidity chamber to keep a constant humidity of 30% RH. Dielectric and impedance spectra were collected in temperature range from 30 to 130 ºC in 10 ºC increments over a frequency of 1-10^7 Hz with ac amplitude of ± 0.05 V. Sample were allowed to soak for 45 minutes at each temperature before measurements were performed.

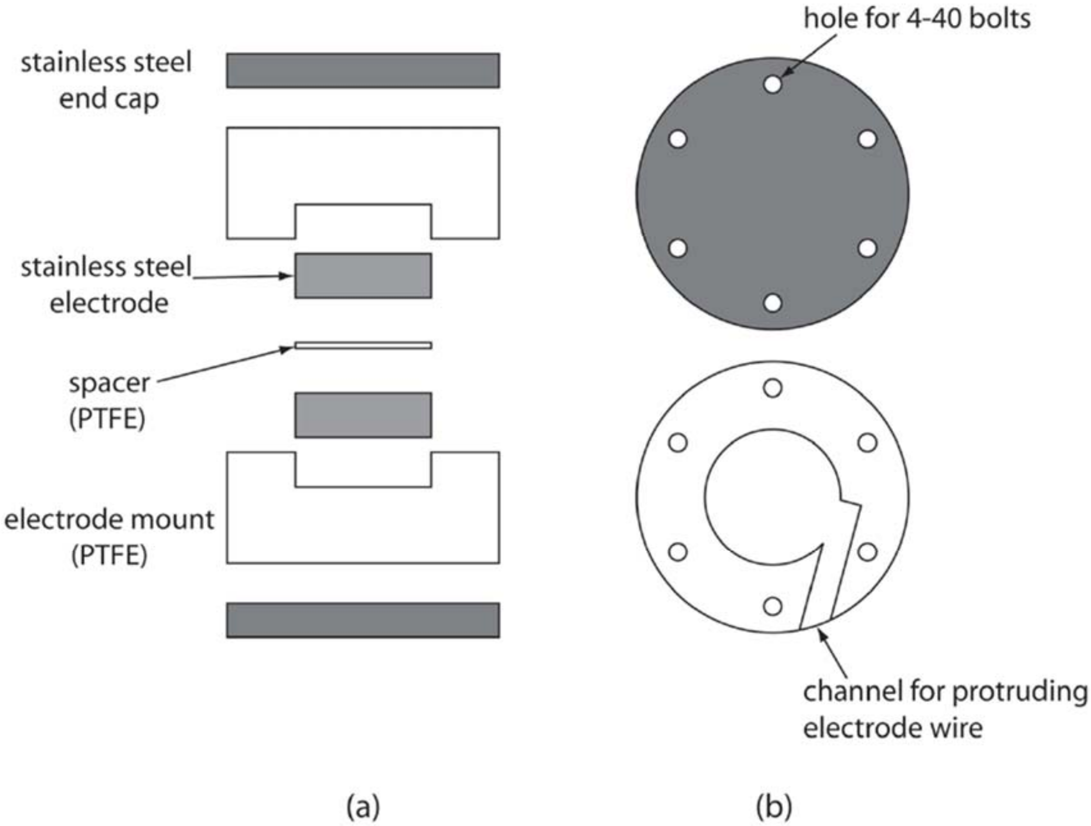

Figure 2-3: a) Side view of the 2-electrode cell used in DRS measurements. b) Top view of the stainless-steel cap and PTFE electrode mount.

CHAPTER THREE

Tetraalkylphosphonium Alkylsulfate Ionic Liquids

1. Material Purity

During the synthesis of ILs using halogenated starting material (Scheme 3-1), residual halide and water may remain in the in the final products, which can have an impact on all measured thermal and transport properties.[1] The purity of the final product was measured with ion chromatography (IC) to detect the presence of residual Cl^-, with < 100 ppm (µg Cl^-/g IL) found in each of the nine samples. In addition, ^{1}H NMR Spectroscopy was performed with special attention paid to alkyl sulfate α protons and phosphonium α protons at 3.98 and 2.25 ppm, respectively (Figure 3-1). In all cases these peaks integrated at ~2 and ~8, respectively, as expected. The purity our synthesized ILs, then, was estimated to be above 98%, based on both IC and ^{1}H NMR.

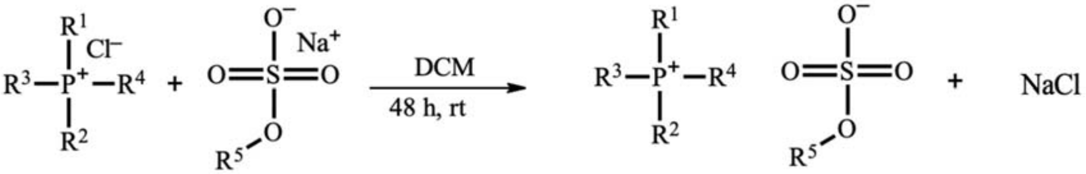

Scheme 3-1: General synthesis of ILs.

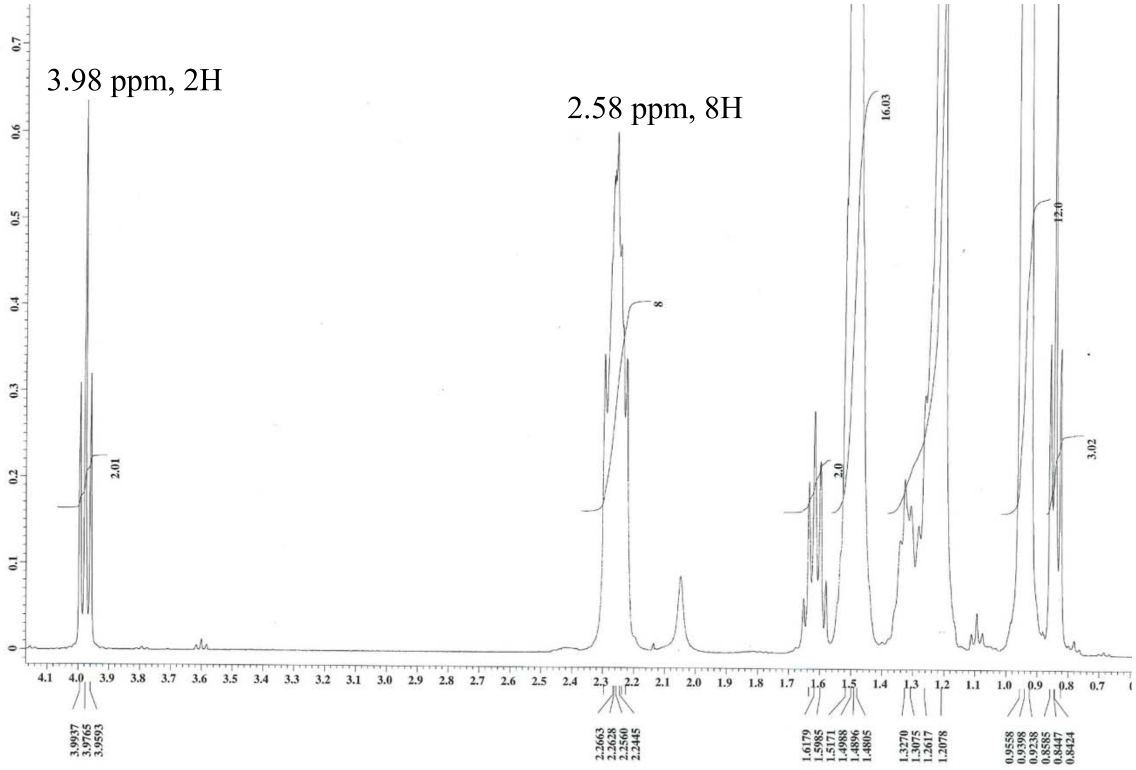

Figure 3-1: ^{1}H NMR spectrum of [tbP$^+$][tds$^-$] in chloroform.

2. Transport Properties

The properties of all ILs were measured over a temperature range of 25 to 80 ºC. Also, all measurements were performed within the same batch to reduce error. Seven of the nine ILs were liquids at room temperature except for [tbtdP$^+$] [dds$^-$] and [tbtdP$^+$] [tds$^-$], which had melting points just above room temperature, at ~ 35 and 37 ºC, respectively.

2.1 Density

An Anton Paar DMA 4100 was used to measure the densities of the synthesized ILs. Density decreased linearly with respect to temperature. The ILs with the smallest cation [tbP$^+$] had the highest densities, while the largest cation family demonstrated the lowest densities, with the trend as follows: [tbP$^+$] > [tbtdP$^+$] > [thtdP$^+$] (Figure 3-2). At the same time, the densities of the three ILs that had the same cation had an increased density with respect to the anion size in the order of [ds$^-$] > [dds$^-$] > [tds$^-$]. The results obtained illustrated that the smaller sized cations and anions pack more closely due to their smaller volumes, and they should have higher densities than in the larger ILs.

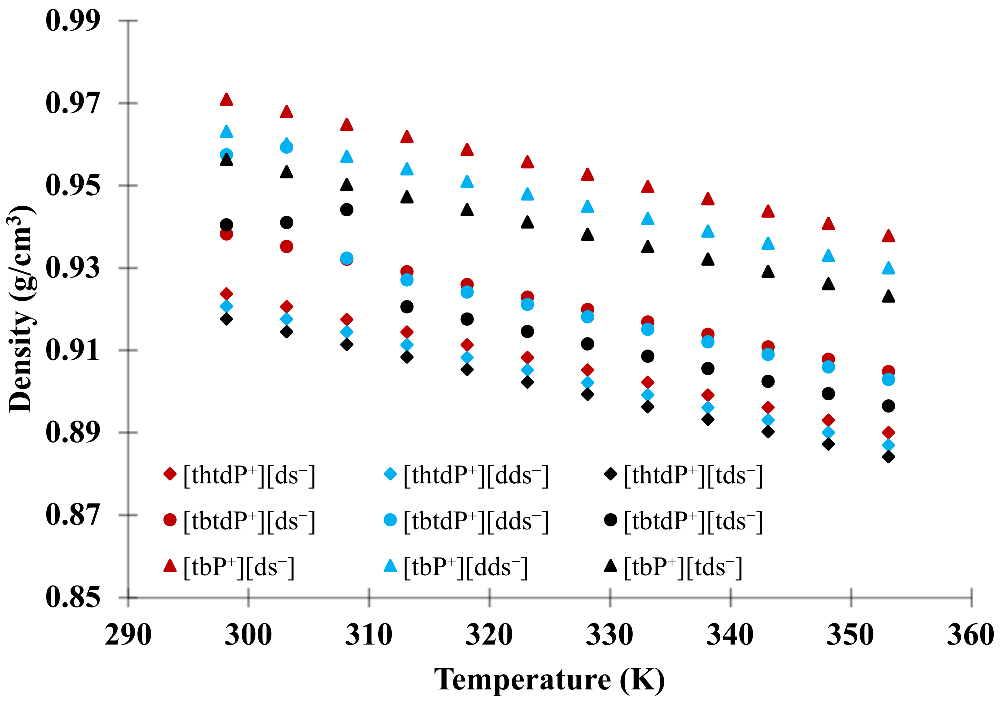

Figure 3-2: Recorded densities of the nine ILs with respect to temperature.

2.2 Viscosity

With viscosity, a slightly different trend was observed. The [tbtdP$^+$] cation family had the highest viscosity among the three, followed by [tdP$^+$] (which was almost the same as [tbtdP$^+$]) then [thtdP$^+$]. The change in pattern could be due to the impact of not just size/packing and ionic interactions but also van der Waals forces. The viscosities of 3 ILs having the same cation showed a trend reverse that of density of an increased viscosity with respect to increasing anion size (Figure 3-3). These results also support the idea that increasing van der Waals interactions are playing a role in viscosity. The results also show that at lower temperature there was a greater difference among the viscosities, where there was slightly larger differences between the ILs at higher temperatures.

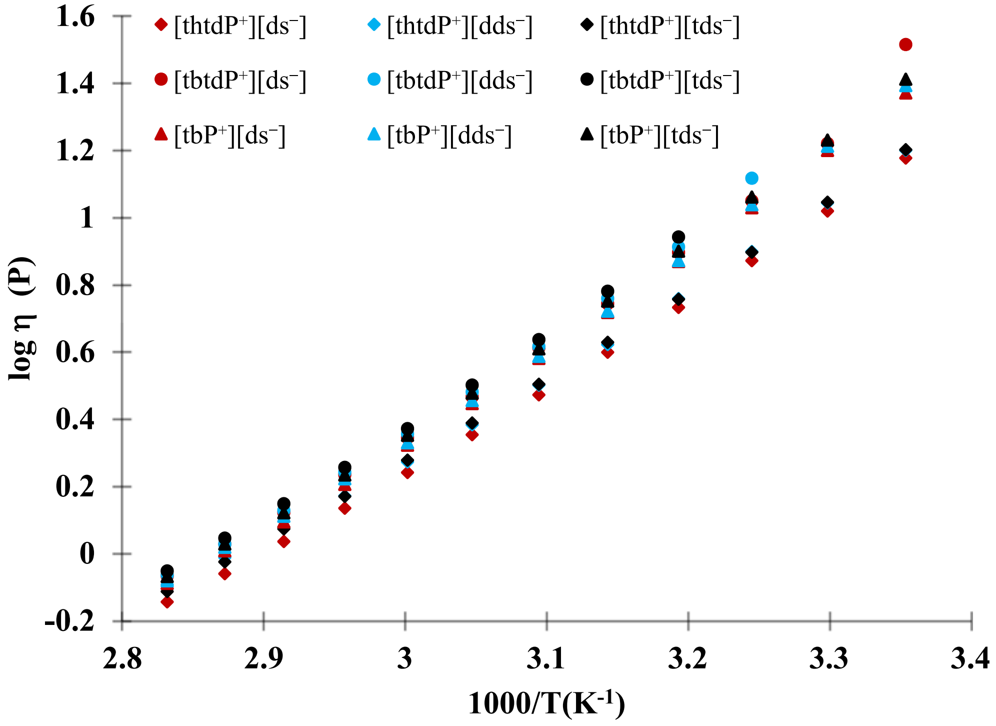

Figure 3-3: Viscosity of ILs with respect to inverse temperature.

2.3 Conductivity

The conductivity of ILs was measured by a custom-built electrode cell (Figure 2-4). Several factors that impact conductivity of ILs should be considered, such as the number of free ions (non-paired, non-clustered) in the IL. In addition, the mobility of the ion plays a significant role as well, with smaller IL ions having higher ionic mobility. Also, temperature is one of the major factors that must be considered, since at higher temperature the kinetic energy increases therefore both mobility of ions and free ions increase giving rise to higher conductivity. The results showed that the smaller sized ILs had the highest conductivity due to having greater mobility compared to the larger ILs. Also, ILs that contained longer alkyl chains (enhanced van der Waals interactions) are likely to have greater numbers of ion pairs and clusters (Figure 3-4).

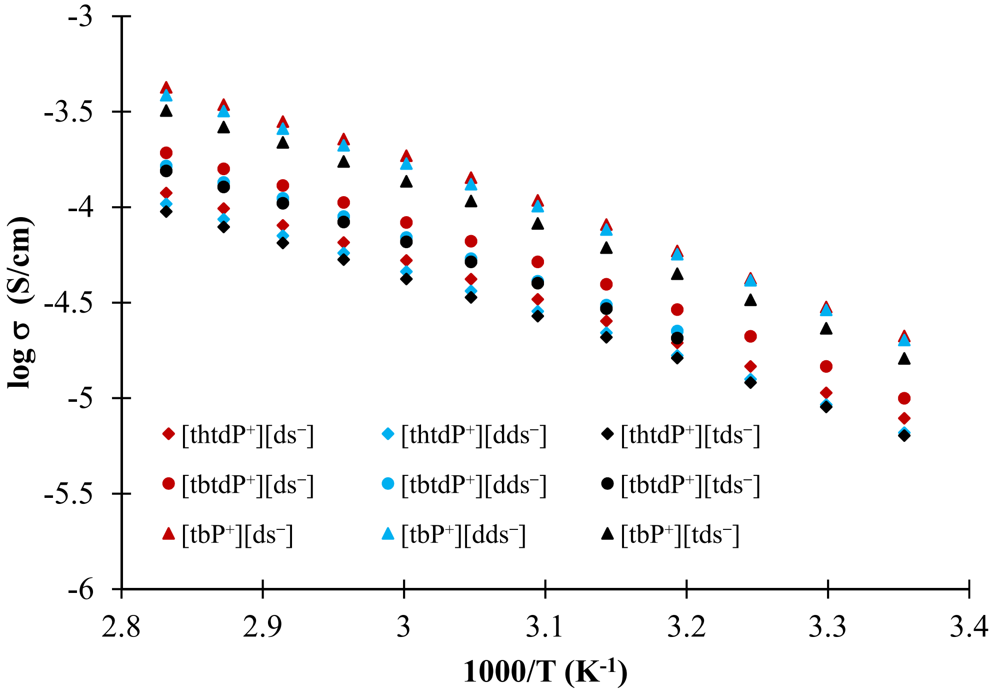

Figure 3-4: Conductivity of ILs with respect to temperature.

A Walden plot[2] was utilized to summarize the relationship between the conductivity, density and viscosity according to the following equations:

$$\Lambda\eta = \text{constant} \tag{3-1}$$

$$\Lambda = \sigma M/\rho \tag{3-2}$$

where Λ is the molar conductivity of the IL (S $cm^{-1}mol^{-1}$), η is the IL viscosity (P), σ is the IL conductivity (S/cm), M is the molecular weight of the IL (g/mol), and ρ is the IL density (g/cm^3). For a better indication of the relative number of mobile charge carriers in an IL, the molar conductivity was used instead of the absolute conductivity (Figure 3-5). In the same Walden plot, the ILs are compared to aqueous KCl as an "ideal" electrolyte solution, where the KCl is assumed to be fully ionized and no ionic interactions are present (i.e., all ions participate individually in conductivity). ILs closer to the KCl line have higher free ion populations (lower "iconicity") and vice versa.

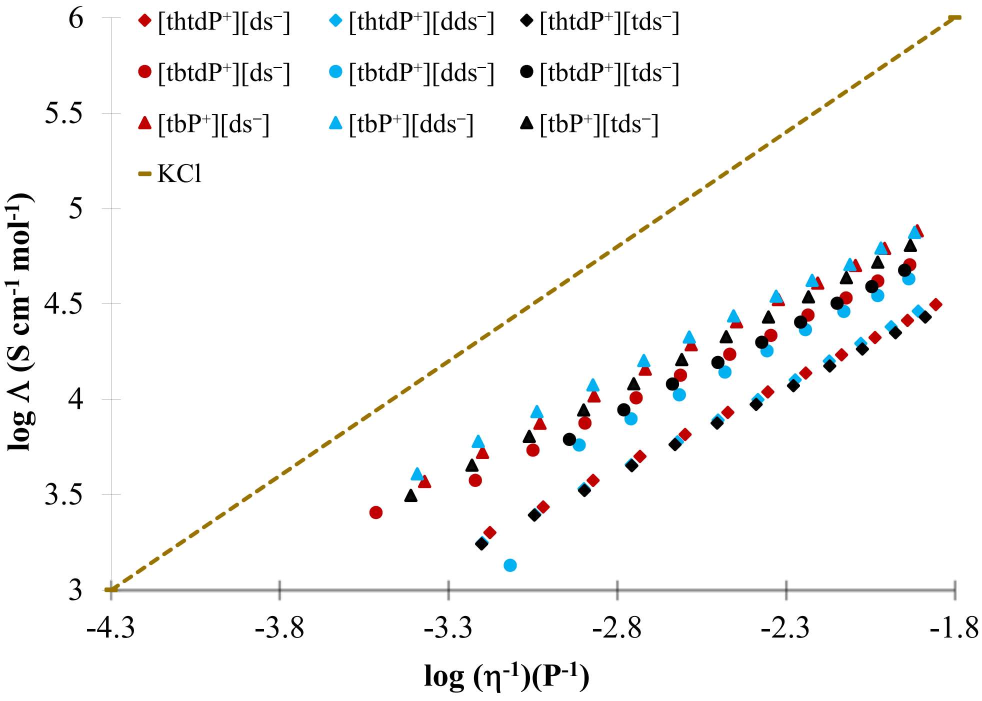

Figure 3-5: Walden Plot

We claimed that smaller sized ILs would have stronger ionic interactions, than larger size ILs, with the trend as follows: [tbP^+] > [$tbtdP^+$] > [$thtdP^+$]. Although the larger size ILs exhibit weaker ionic interactions, they have stronger van der Waals intermolecular forces that form between the alkyl chains. Therefore, the large ILs would be held together more strongly as associated ion pairs and clusters as what was observed in the Walden plot above.

2.4 Discussion

The size of cations and anions significantly impacted IL conductivity, viscosity, and density, because size plays a significant role in volume, the ability to pack, mobility, and ionic interactions. More specifically, the size of the cation itself had the most significant impact with anion size having only a minor effect on the measured properties. The results showed that properties of ILs containing the same cation were clustered. The net change in properties with respect to anion followed a noticeable trend, but that was not as significant as for cations.

While patterns related to the ion size were noted, size/ionic interactions were insufficient in explaining for the overall trends. Therefore, the ability of the ion to interact via van der Waals forces also was important. The measurement outcomes, then, supported the hypothesis that cation and anion ionic interactions are not the only factor that can impact the properties of the ILs, van der Waals forces between the alkyl chains also contribute. For example, among the nine tested ILs, [tbP^+] ILs showed greater packing efficiency and should have stronger ionic interaction but possessed the weakest van der Waals forces due to shorter alkyl chains. On the other hand, weaker ionic interaction and poorer packing, but higher van der Waals forces should be present in ILs containing [$thtdP^+$] cations.

2.5 Summary

The work described in this chapter focused on the impact of both ionic interactions and intermolecular forces, such as van der Waals, on the physicochemical properties (conductivity, viscosity, and density) of nine tetraalkylphosphonium alkylsulfate ILs. The nine ILs were synthesized, and the final product purity was above 98% according to ^{1}H NMR spectroscopy and IC. Conductivity, viscosity, and density measurements were obtained over a temperature range of 25 - 80 ºC. In the case of density, ILs with the smallest cation (tbP$^+$) had the highest density, while the largest cation family demonstrated the lowest density. At the same time, the densities of the 3 ILs that had the same cation had an increased density with respect to the anion size.

With viscosity, a slightly different trend was observed, the tbtdP$^+$ cation family had the highest viscosity among the three, followed by tbP$^+$ (which was almost the same as tbtdP$^+$) then thtdP$^+$. The change in pattern could be due to the impact of not just of size/packing and ionic forces but also van der Waals forces. Conductivity was highest for the smallest ILs (tbP) while the lowest conductivity was reported for the largest IL (thtdP). Within the same cation group, higher conductivity was measured for the smallest anion size. Walden plot analysis revealed the ionicity of the ILs compared to ideal conductive aqueous (KCl).

CHAPTER FOUR

Thiol-ene-based Polymerized Ionic Liquids in 3D Printing

1. Curing Rate

The photoinitiator is one of the most important elements of the thiol-ene photopolymerization. Decomposition of photoinitiator into a radical occurs when it absorbs a photon. The utilized 3D printer has a 405 nm laser so the photoinitiator must absorbs a photon around this wavelength. Phenylbis(2,3,6-trimethylbenzoyl) phosphine oxide (PI) or IRGACURE® 819 is a commercially available initiator that absorbs well at 405 nm. Furthermore, due to the poor resolution of the printed pieces using neat the thiol-ene resin, Sudan I was chosen as an additive to absorb scattered laser light and improve resolution. Sudan I absorbs strongly between 376 and 486 nm, which make it a suitable anti-scattering agent.[17]

The curing rate of the thiol-ene resin with respect to Sudan I concentration (0%, 0.02%, 0.05%, 0.1%, and 0.2 % w/w) was tested by two different methods, laser spot curing and photorheology. In general, the results of both methods showed an increase in the curing time as Sudan I concentration increased. The laser spot curing was performed using a 50 mW, 405 nm laser pointer to cure 1:1 and 1:2 thiol-ene with different Sudan I concentrations. Then, thicknesses of the cured pieces were measured with respect to the exposure, which is irradiance (mW/mm^2) times exposure time (s). From the results, (Figure

4-1 and Figure 4-2) it was determined that curing a 100 µm thick layer in the printer should be feasible at concentrations of 0.02 and 0.05 % w/w Sudan I in the thiol-ene resin. This conclusion assumes a printer exposure of ~0.4 mJ/mm^2.

Photorheology was performed on a TA Instruments Discovery Hybrid Rheometer HR-2 equipped with UV curing accessory at 4.5 and 22.6 mW/cm^2 lamp irradiance. An example of the data collected is shown in Figure A-1. Overall, the gel point times (the time at which storage and loss modulus cross over, i.e., the material transitions from liquid-like behavior to solid-like behavior) showed a logarithmic dependence on Sudan I concentration. For example, the 1:1 thiol-ene with no Sudan I had a gel point of 12.48 s at 4.5 mW/cm^2 (exposure of 0.562 mJ/mm^2), whereas the same composition of thiol-ene with 0.1% w/w Sudan I had a gel point of 81.22 s under the same conditions (Figure 4-3).

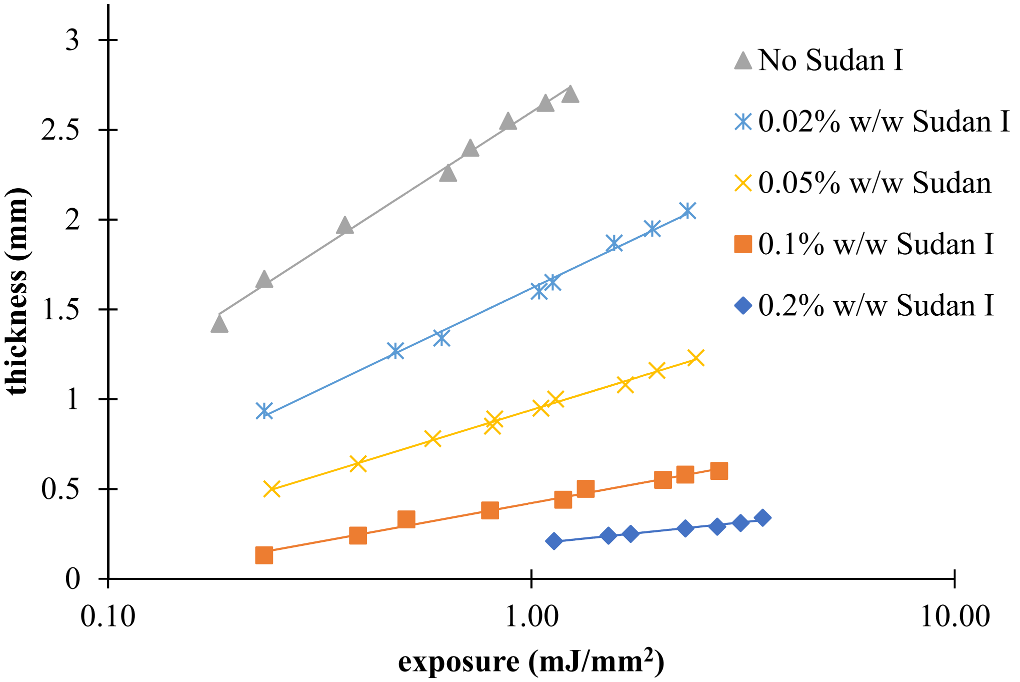

Figure 4-1: Laser spot curing of the 1:1 thiol-ene with different % w/w Sudan I.

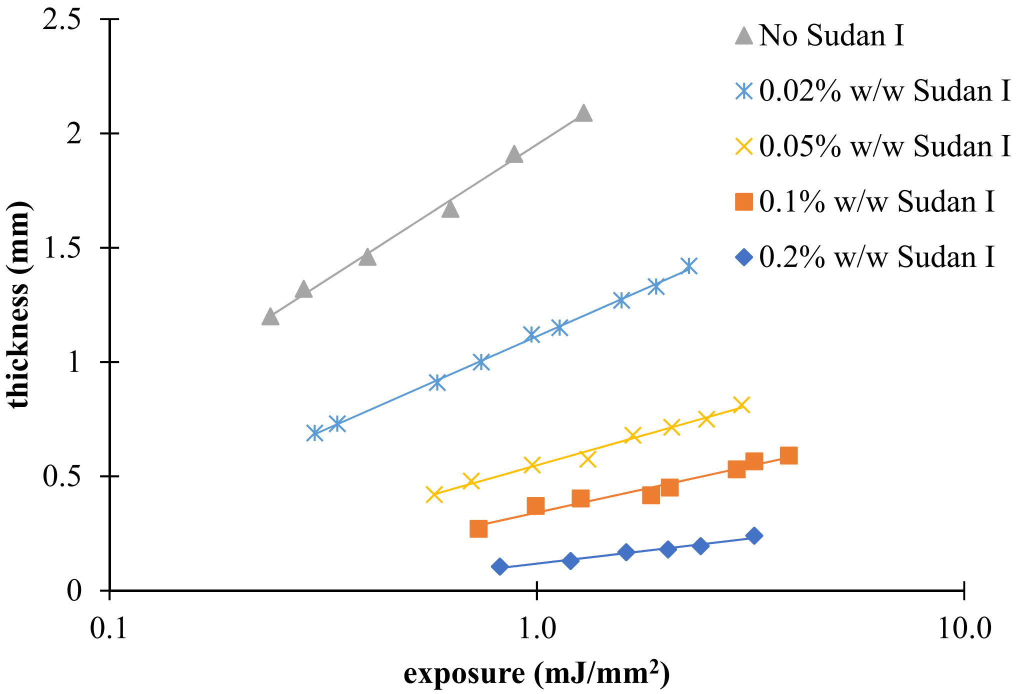

Figure 4-2: Laser spot curing of the 1:2 thiol-ene with different % w/w Sudan I.

It should be noted that these gel point times were determined for a 200 µm thick layer of monomer resin. The gel point test further helped us to determine the right concentration of Sudan I that can be added to a 3D printing resin. In general, the 0.1% and 0.2% w/w Sudan I polymers did not gel fast enough with respect to the laser intensity used in the 3D printer. So, again, we concluded that either 0.02 or 0.05% w/w Sudan I would be acceptable. However, when a 1:1 thiol-ene PIL resin containing 0.05% Sudan I was examined as a 3D printing resin, the printed pieces did under-cure to the extent that the layers did not adhere to one another, i.e. they peeled apart. Therefore, all other printing was performed using resins with 0.02% w/w Sudan I.

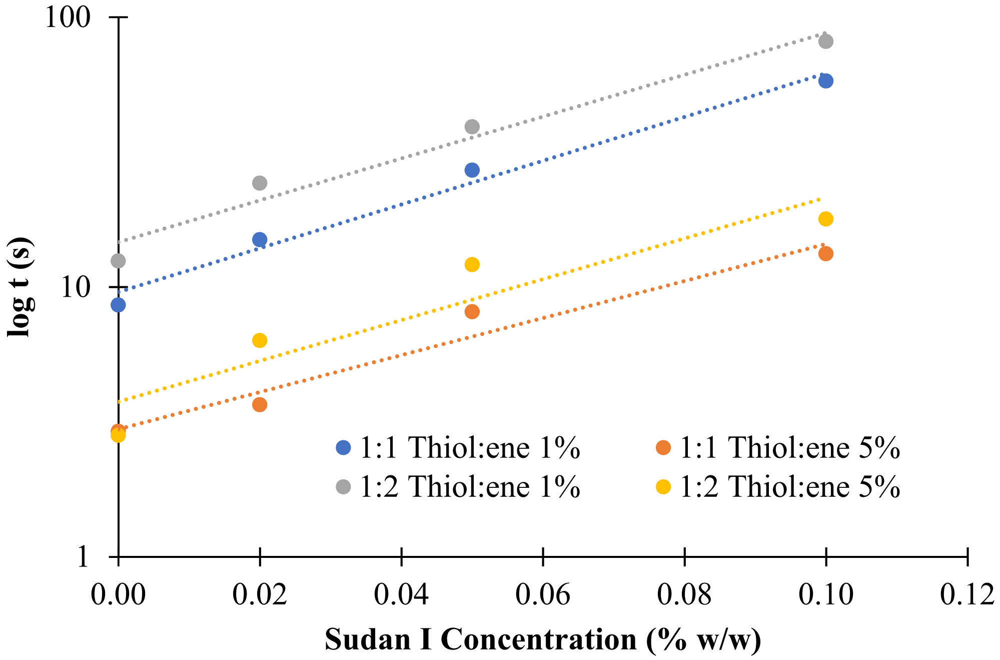

Figure 4-3: Photorheology of 1:1 and 1:2 thiol:ene at 1% and 5% lamp intensities.

2. Thermal and Mechanical Analysis

2.1 Differential Scanning Calorimetry (DSC)

Thermal glass transition temperature (T_g) was measured by DSC; an example of the data collected is shown in Figure A-2. The average of two replicates of the second heating cycle was calculated for each thiol-ene polymer with Sudan I as shown Table 3-1. The first heating cycle was performed for the removal of residual solvent and to erase the thermal history of the polymer. For all 1:1 thiol-ene with different Sudan I concentrations and for UV cured and 3D printed objects, the average T_g value was -24.55 ± 1.4 ºC. This standard deviation is within the uncertainty for the instrument, so T_g for these samples are basically the same. On the other hand, the 1:2 thiol-enes resin averaged a T_g value of -12.38 ± 3.3 ºC, which is approximately twice the T_g value for 1:1 thiol-ene due to the higher degree of network cross-linking. The 1:2 thiol-ene T_g range is slightly greater than the accepted uncertainty for DSC, hence the values are probably not the same for different % w/w Sudan I. In fact, a trend of decreasing T_g with increasing % w/w Sudan I is observed. Therefore, Sudan is likely reducing network curing/crosslinking.

2.2 Dynamic Mechanical Analysis (DMA)

The DMA was used to characterize the mechanical properties of the thiol-ene polymers containing Sudan I; example data is shown in Figures A-3 and A-4. In the DMA, two pieces of data were obtained: tan δ max (mechanical T_g) and storage modulus ($E^{'}$) at 100 °C, which is an indicator of network crosslinking. The data were obtained at a constant strain (frequency = 1 Hz) and an average from the second heating of two trials for each polymer (Table 3-1). The average tan δ max T_g value for 1:1 thiol-ene samples was -12.38 ± 2.6 °C. In general, DSC glass transition (T_g) values were lower than the obtained DMA tan δ max T_g, as the two instruments are measuring T_g via different phenomena – heat flow versus tensile deformation. The results showed that 3D printed thiol-ene polymer had very similar tan δ max T_g compared to UV cured polymers. This indicate that the interaction between each layer of 3D printed polymer had little impact on the tensile mechanical properties.

Storage modulus ($E^{'}$) values also were obtained to investigate the impact of the Sudan I addition on the mechanical properties of the thiol-ene resin. E’ values were in the expected ranges for the thiol-ene polymer networks according to a previously published article by our group.[6] Apparent crosslinked density (ν_c) was from the rubbery plateau region of the storage modulus curve was calculated using the following equation:

$$\nu_c = E' / 3RT \qquad (4\text{-}1)$$

The crosslink density of the 1:1 thiol-ene was observed to change very little for all compositions, which indicates that the addition of Sudan I had no significant impact on the polymer crosslinking. In 1:2 thiol-enes, though, E' decreased with increasing Sudan I concentration. The difference in behavior is likely due to the fact that 1:2 is the stoichiometric ratio for the polymer and should be fully crosslinked; therefore, Sudan I is limiting some of the crosslink formation.

Table 4-1: DSC and DMA data for thiol-ene polymers containing Sudan I.

thiol:ene ratio	**% Sudan I**	**DSC T_g (°C)**	**DMA tan δ max T_g (°C)**	**DMA E' @ 100 °C (MPa)**	**ν_c x 10^{-4} (mol/cm^3)**
1:1	0.00	-25.9	-11.2	0.654	0.70
1:1	0.02	-25.4	-14.1	0.801	0.86
1:1	0.05	-23.0	-14.1	0.984	1.06
1:1	0.10	-22.7	-13.7	1.027	1.10
3DP 1:1	0.00	-24.8	-8.2	0.594	0.64
3DP 1:1	0.02	-25.5			
1:2	0.00	-9.8	2.0	5.183	5.57
1:2	0.02	-8.6	7.3	6.846	7.36
1:2	0.05	-15.9	-7.8	4.519	4.86
1:2	0.10	-16.5	-8.2	4.234	4.55
3DP 1:2	0.00	-10.4	2.7	5.172	5.56
3DP 1:2	0.02	-13.1	4.5	3.827	4.11

2.3 Thermogravimetric Analysis (TGA)

The thermal degradation temperature (T_{onset} and $T_{d5\%}$) of the 1:1 and 1:2 thiol-ene polymers with different Sudan I concentrations were determined using TGA (Table 4-2 and Figure A-5). The results indicated that all of the polymers, regardless of the thiol:ene ratio, concentration of Sudan I added, and whether UV cured or 3D printed had approximately the same decomposition temperature. For instance, $T_{d5\%}$ was 342.2 ± 2.1 °C (Table 4-2). Generally, the temperature uncertainty for TGA under the conditions used is approximately ± 5.0 °C. Therefore, the $T_{d5\%}$ are not statistically different.

Table 4-2: TGA data for thiol-ene polymers containing Sudan I.

Thiol:ene ratio	% Sudan I	TGA T_{onset} (°C)	TGA $T_{d5\%}$ (°C)
1:1	0.00	356	344
1:1	0.02	342	334
1:1	0.05	341	338
1:1	0.10	348	340
3DP 1:1	0.00	356	344
3DP 1:1	0.02	346	334
1:2	0.00	356	346
1:2	0.02	342	343
1:2	0.05	341	340
1:2	0.10	344	343
3DP 1:2	0.00	356	345
3DP 1:2	0.02	342	342

2.4 Dielectric Relaxation Spectroscopy (DRS)

DRS was performed to measure the conductivity of the thiol-ene networks. The thiol-ene samples were sandwiched between two stainless steel electrodes, ac potential (±10 mV) was applied, and impedance/dielectric behavior was obtained as a function of frequency. Complex dielectric constant was used to calculate the dc conductivity of the sample over a range of temperatures (30 to 130 °C, 10 °C increments). The evaluation of the ionic conductivity of the thiol-ene polymer networks was performed collecting frequency-dependent dielectric spectra of each of the thiol-ene polymer.[24] The dielectic loss spectra (ε'') was converted to the real conductivity (σ') using the following equation:

$$\sigma' = \varepsilon''\varepsilon_o\omega \qquad (4\text{-}2)$$

where ε_o is vacuum permittivity and ω is angular frequency in rad/s. Then, from the frequency independent plateau region of the real conductivity spectra, the direct current conductivity values (σ) were taken to be the plateau value.

The obtained conductivities were essentially the same within each thiol-ene ratio regardless of Sudan I concentration, or whether 3D printed or UV cured. Any small differences observed in Figures 4-4 and 4-5 could be attributed to small differences in T_g (Table 4-1).

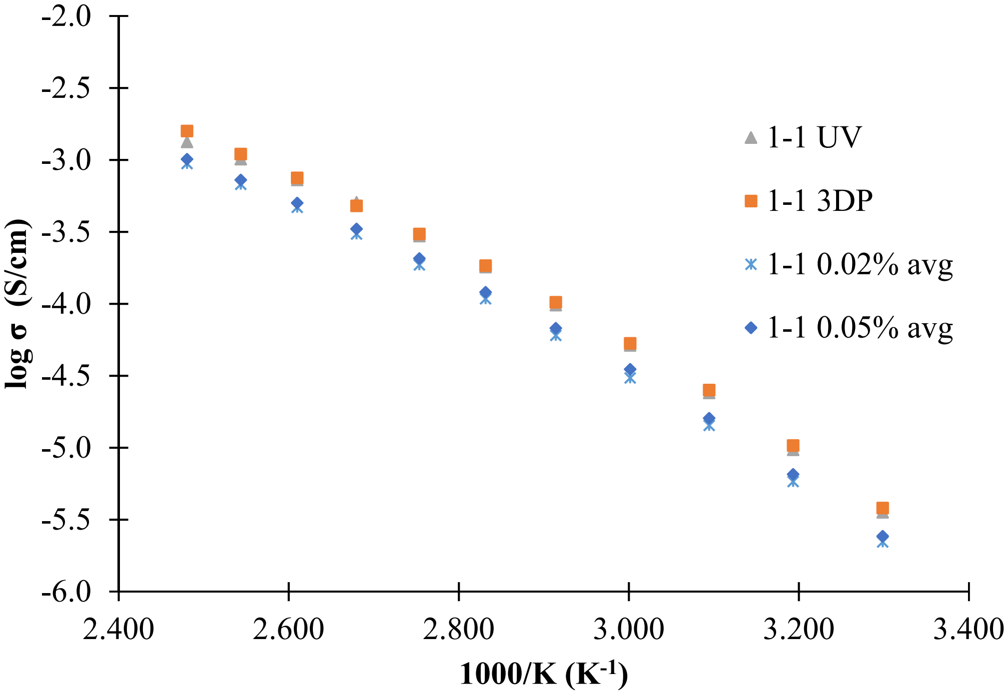

Figure 4-4: Ionic conductivity of UV cured and 3D printed 1:1 thiol-ene polymers.

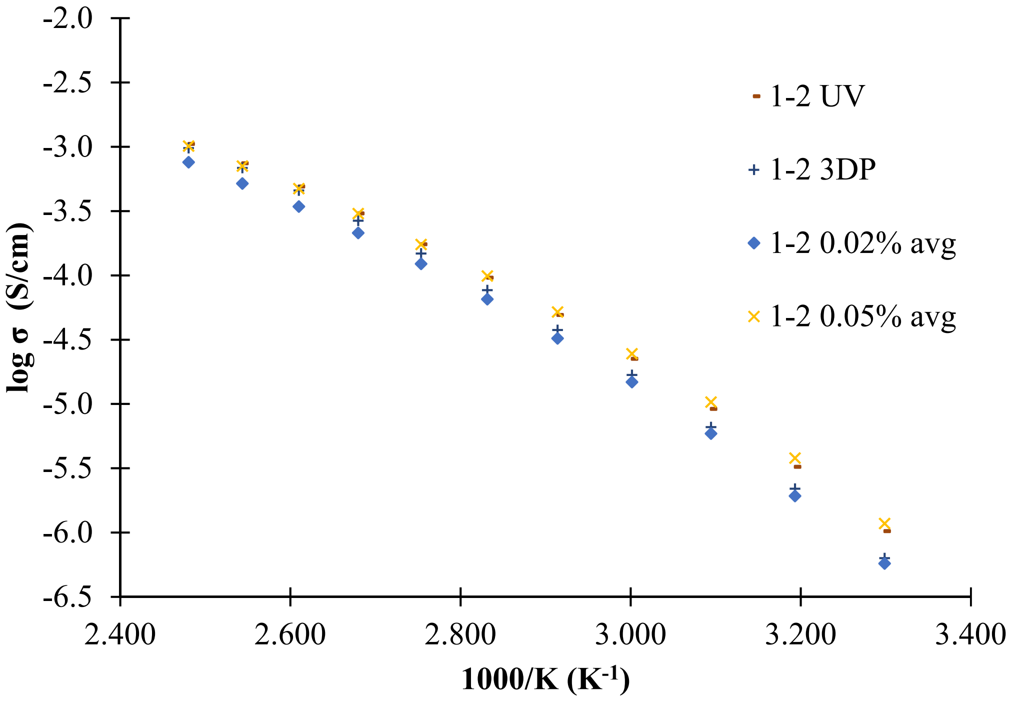

Figure 4-5: Ionic conductivity of UV cured and 3D printed 1:2 thiol-ene polymers.

3. Resolution Evaluation

For evaluating resolution, squares of known dimensions were printed, and the actual and specified dimensions were compared. For example, squares prepared a 1:2 thiol-ene network containing no Sudan I were found to be between 20 - 28% bigger than specified (“overgrowth”), while the same 1:2 polymer containing 0.02% Sudan showed improved resolution having 12 to 17% overgrowth (Figure 4-6). Results of overgrowth from various square dimensions is shown in Table 4-3. The overall reduction in overgrowth with Sudan I present illustrates that this addition can be successfully used in thiol-ene resins for 3D printing.

Table 4-3: Overgrowth (OG) measurements of printed squares. The indicated dimension is the size of the internal square. All outside square dimensions were 5 mm.

	OG (mm)	% of side width	OG (mm)	% of side width
	1:2 neat		*1:2 + 0.02% w/w Sudan I*	
4 mm	0.187	37.3	0.137	27.5
3 mm	0.279	27.9	0.169	16.9
2 mm	0.352	23.4	0.186	12.4
1 mm	0.401	20.1	0.246	12.3

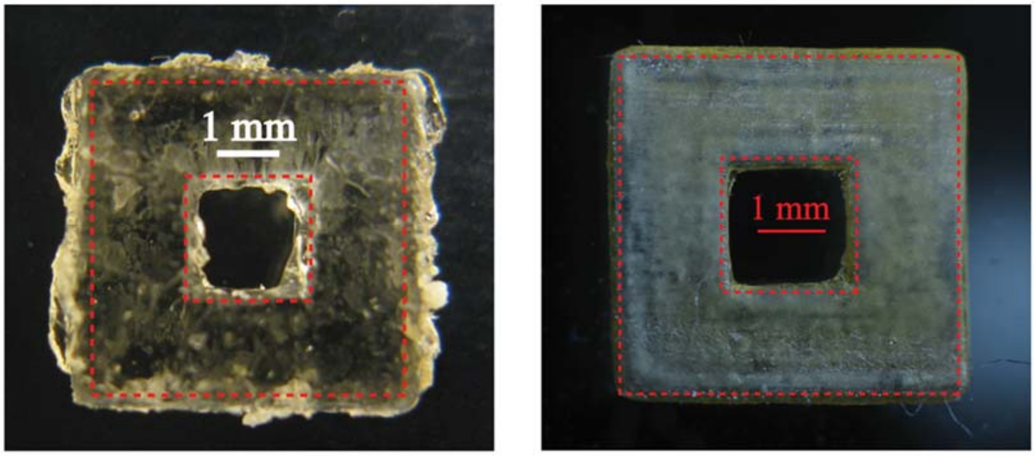

(a) (b)

Figure 4-6: (a) 5 mm square with 2 mm opening printed using 1:2 thiol-ene with no Sudan I, (b) 5 mm square with 2 mm opening printed using 1:2 thiol-ene containing 0.02% Sudan I.

4. Summary

This project involved improving the resolution of parts created from a polymerized IL in a commercial 3D printer. Previous preliminary work performed by our group showed that thiol-ene PILs containing PTMP, bisallylimidazolium NTf_2, and a phosphine oxide-based photoinitiator could be successfully employed as a 3D printing resin. However, the resolution of the printed pieces was not satisfactory due to light scattering within the resin. In this study the main focus was to enhance the resolution by adding an anti-scattering agent (Sudan I). Also, the possible impacts on thermal, mechanical, and conductive properties by Sudan I were studied.

Photorheology and laser spot curing tests were performed to examine the curing behavior of the new resins. These tests aided the identification of the appropriate concentration of Sudan I for 3D printing. In the end, adding Sudan I at 0.02% w/w improved the resin, which printed with better resolution. A 1:2 thiol-ene polymer with no Sudan showed 20 - 28% overgrowth, while the same polymer containing 0.02% Sudan showed improved resolution with between 12 and 17% overgrowth. In addition, TGA, DMA, DSC, and DRS results showed that there were no significant changes in the thermal, and conductive properties when Sudan I was added to the resin.

5. Future Directions

Our group is interested in building a custom 3D printer with adjustable light intensity and focusing as a future project. The commercial 3D printer had a fixed laser intensity, and in this study, we were forced to rely only on changing the chemistry of the resin to enhance the resolution. Having a 3D printer with more flexible settings would allow us to perform a wider range of experimental prints.

REFERENCES

1. Welton, T. Room-Temperature Ionic Liquids. Solvents for Synthesis and Catalysis. *Chem. Rev.* **1999**, *99*, 2071–2084.
2. Choi, U. H.; Middleton, L. R.; Soccio, M.; Buitrago, C. F.; Aitken, B. S.; Masser, H.; Wagener, K. B.; Winey, K. I.; Runt, J. Dynamics of Precise Ethylene Ionomers Containing Ionic Liquid Functionality. *Macromolecules* **2015**, *48*, 410–420.
3. Hendriks, B.; Waelkens, J.; Winne, J. M.; Prez, F. E. D. Poly(Thioether) Vitrimers via Transalkylation of Trialkylsulfonium Salts. *ACS Macro Lett.* **2017**, *6*, 930–934.
4. Lin, B.; Cheng, S.; Qiu, L.; Yan, F.; Shang, S.; Lu, J. Protic Ionic Liquid-Based Hybrid Proton-Conducting Membranes for Anhydrous Proton Exchange Membrane Application. *Chem. Mater.* **2010**, *22*, 1807–1813.
5. Mjalli, Farouq S. Tetrabutylammonium Chloride Based Ionic Liquid Analogues and Their Physical Properties. *J. Chem. Eng.* **2014**, *59*, 2242–2251.
6. Rhoades, T. C.; Wistrom, J. C.; Johnson, R. D.; Miller, K. M. Thermal, Mechanical and Conductive Properties of Imidazolium-Containing Thiol-Ene Poly(Ionic Liquid) Networks. *Polymer* **2016**, *100*, 1–9.
7. Park, M. J.; Choi, I.; Hong, J.; Kim, O. Polymer Electrolytes Integrated with Ionic Liquids for Future Electrochemical Devices. *J. Appl. Polym. Sci.* **2013**, *129*, 2363–2376.
8. Wang, R.; Lowe, A. B. RAFT Polymerization of Styrenic-Based Phosphonium Monomers and a New Family of Well-Defined Statistical and Block Polyampholytes. *J. Polym. Sci.* **2007**, *45*, 2468–2483.

9. Hoyle, C. E.; Lee, T. Y.; Roper, T. Thiol-Enes: Chemistry of the Past with Promise for the Future. *Polymer. Sci.* **2004**, *42*, 5301–5338.
10. Yuan, J.; Antonietti, M. Poly(Ionic Liquid)s: Polymers Expanding Classical Property Profiles. *Polymer* **2011**, *52*, 1469–1482.
11. Kade, M. J.; Burke, D. J.; Hawker, C. J. The Power of Thiol-Ene Chemistry. *J. Polym. Sci.* **2010**, *48*, 743–750.
12. Vestberg, R.; Piekarski, A. M.; Pressly, E. D.; Van Berkel, K. Y.; Malkoch, M.; Gerbac, J.; Ueno, N.; Hawker, C. J. A General Strategy for Highly Efficient Nanoparticle Dispersing Agents Based on Hybrid Dendritic Linear Block Copolymers. *J. Polym. Sci. Pol. Chem.* **2009**, *47*, 1237–1258.
13. Ligon, S. C.; Liska, R.; Stampfl, J.; Gurr, M.; Mülhaupt, R. Polymers for 3D Printing and Customized Additive Manufacturing. *Chem. Rev.* **2017**, *117*, 10212–10290.
14. Yang, G.; Kristufek, S. L.; Link, L. A.; Wooley, K. L.; Robertson, M. L. Synthesis and Physical Properties of Thiol–Ene Networks Utilizing Plant-Derived Phenolic Acids. *Macromolecules* **2015**, *48*, 8418–8427.
15. Gross, B.; Lockwood, S. Y.; Spence, D. M. Recent Advances in Analytical Chemistry by 3D Printing. *Anal. Chem.* **2016**, *89*, 57–70.
16. Ambrosi, A.; Pumera, M. 3D-Printing Technologies for Electrochemical Applications. *Chem. Soc. Rev.* **2016**, *45*, 2740–2755.
17. Murphy, S. V.; Atala, A. 3D Bioprinting of Tissues and Organs. *Nat. Biotechnol.* **2014**, *32*, 773–785.
18. Ho, C. M. B.; Ng, S. H.; Li, K. H. H.; Yoon, Y.-J. 3D Printed Microfluidics for Biological Applications. *Lab Chip* **2015**, *15*, 3627–3637.

19. Au, A. K.; Huynh, W.; Horowitz, L. F.; Folch, A. 3D-Printed Microfluidics. *Angew. Chem.* **2016**, *55*, 3862–3881.
20. Baden, T.; Chagas, A. M.; Gage, G. J.; Marzullo, T. C.; Prieto-Godino, L. L.; Euler, T. Correction: Open Labware: 3-D Printing Your Own Lab Equipment. *PLoS Biol.* **2015**, *13*.
21. Schultz, A. R.; Lambert, P. M.; Chartrain, N. A.; Ruohoniemi, D. M.; Zhang, Z.; Jangu, C.; Zhang, M.; Williams, C. B.; Long, T. E. 3D Printing Phosphonium Ionic Liquid Networks with Mask Projection Microstereolithography. *ACS Macro Lett.* **2014**, *3*, 1205–1209.
22. Fike. L. Thiol-Ene Polymeric Ionic Liquids: Conductivity and Fabrication by 3D Printing. Honors Thesis, *Murray State University, Murray, KY,* **2017**
23. Wu, L. Visual Detection of Sudan Dyes Based on the Plasmon Resonance Light Scattering Signals of Silver Nanoparticles. *Anal. Chem.* **2006**, *78*, 5570–5577.
24. Tracy, C. A.; Adler, A. M.; Nguyen, A.; Johnson, R. D.; Miller, K. M. Covalently Crosslinked 1,2,3-Triazolium-Containing Polyester Networks: Thermal, Mechanical, and Conductive Properties. *ACS Omega* **2018**, *3*, 13442–13453.

APPENDIX

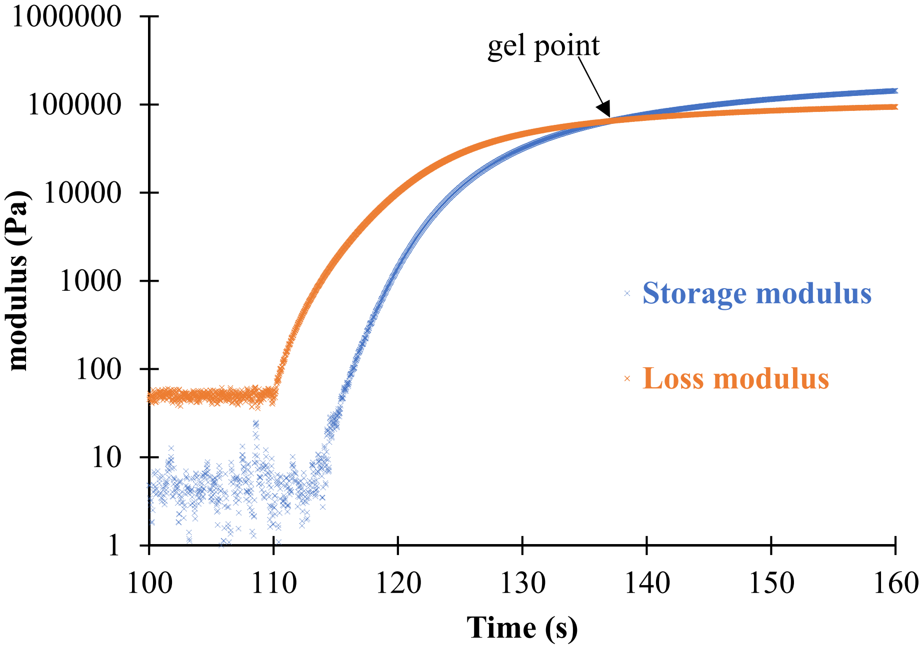

Figure A-1: Photorheology storage and loss modulus crossing (gel point)

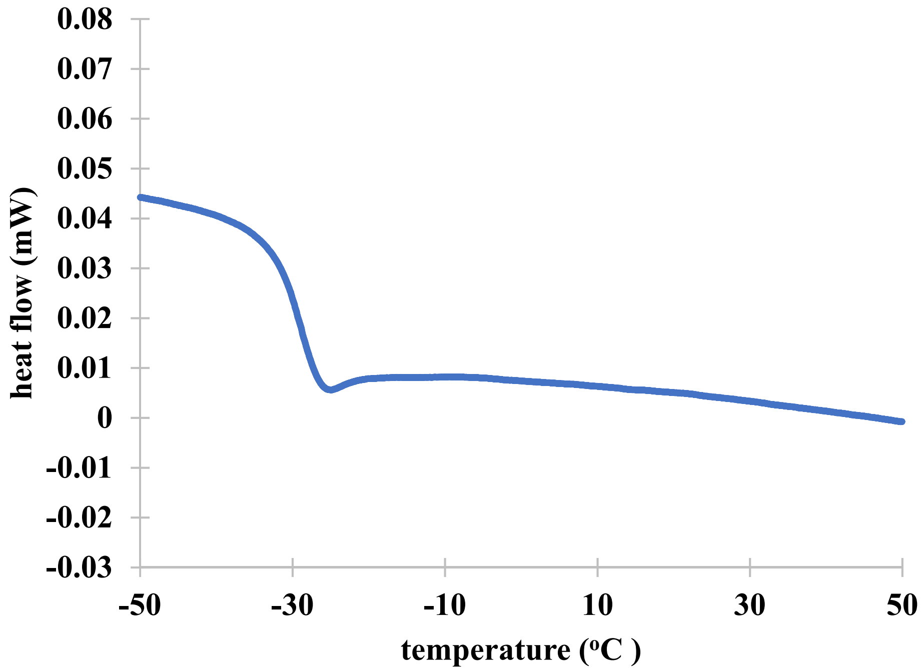

Figure A-2: DSC second heating curve for thiol-ene polymer network.

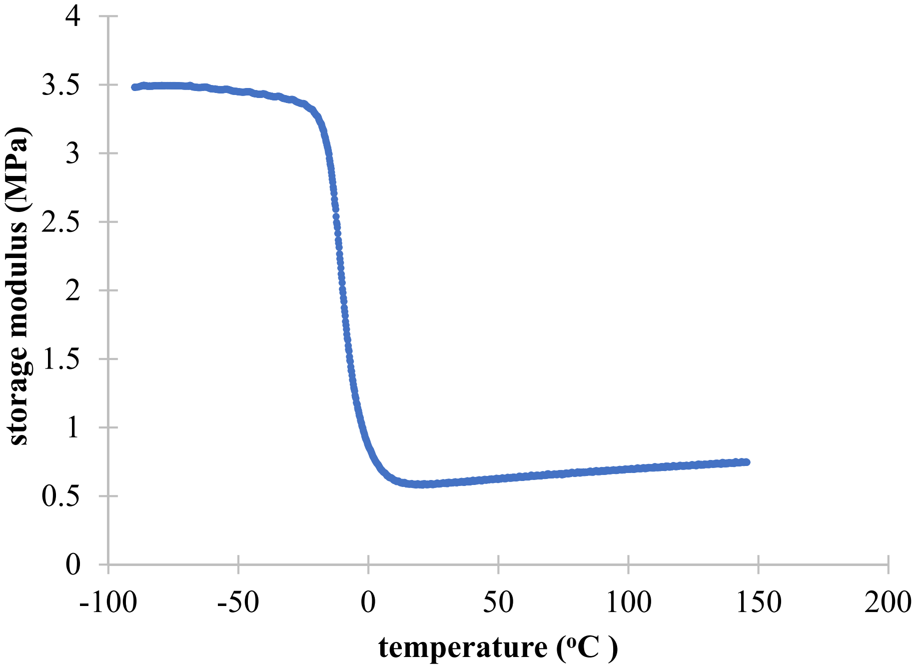

Figure A-3: DMA storage modulus (E') curve for thiol-ene polymer network.

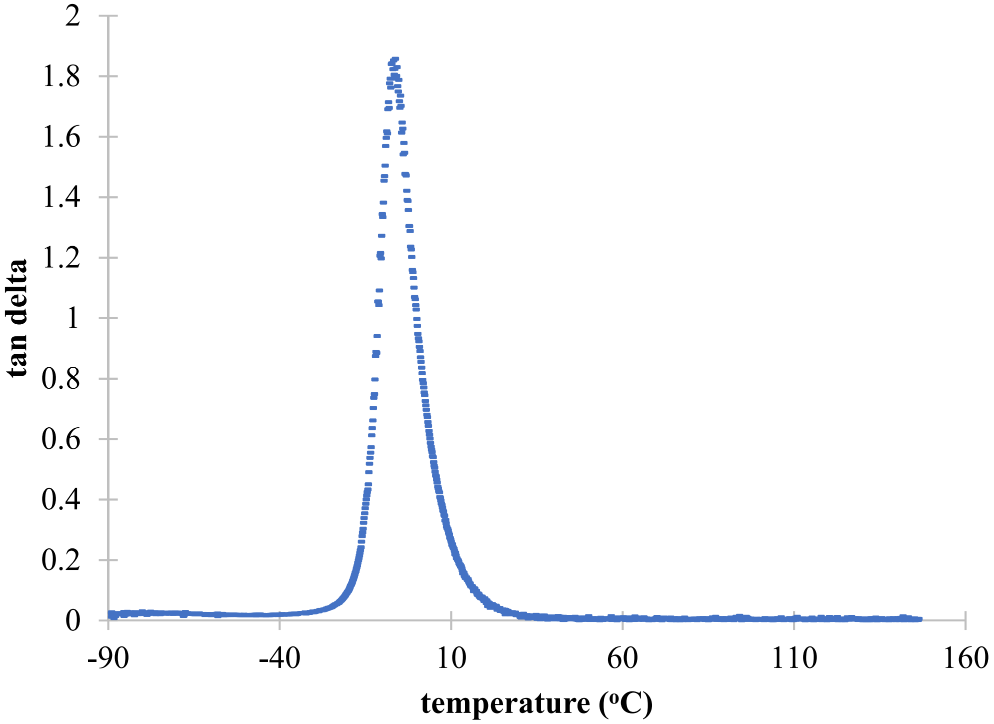

Figure A-4: DMA tan delta curve for thiol-ene polymer network.

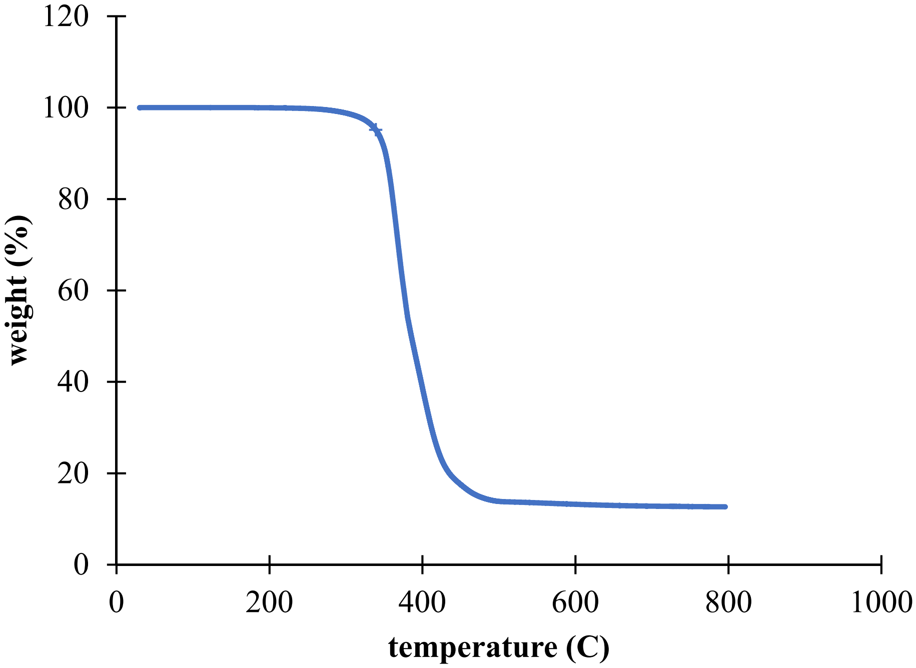

Figure A-5: TGA curve for thiol-ene polymer network.